

Supplemental material for the manuscript titled  
**“Reconstruction of three-dimensional biventricular activation based on 12-lead ECG via patient-specific modeling”**  
by Pezzuto et al.

## **ECG recordings**

The 12-lead ECG was recorded using a clinically available ECG machine (CS200 excellence, Schiller AG) having a sampling rate of 1000/s and an amplitude resolution of 1.0  $\mu$ V. The target QRS complex was isolated from a single beat, with no additional filter applied. The QRS onset and duration were detected manually. A linear detrend was subtracted from the QRS complex to correct the baseline.

## **Cardiac magnetic resonance**

[Cardiac magnetic resonance \(CMR\)](#) data were acquired with a 3T scanner (MAGNETOM Skyra, Siemens Healthcare, Erlangen, Germany) with 36-channel torso coils. ECG-triggered, steady-state free precession cine CMR were acquired in the 2-, 3- and 4-chamber orientation and in a sequence of short-axis slices covering the ventricles (temporal resolution 25 to 40 ms, voxel size 1.2 mm  $\times$  1.2 mm  $\times$  8 mm.) A series of ultra-fast GRE sequences (axial, coronal and sagittal) were obtained to describe the torso anatomy and the location of surface electrodes. Scar detection was performed on a short-axis sequence 7 to 12 min after gadolinium injection (gadobutrol, 0.2 mmol/kg body weight).

## **Electroanatomic mapping**

The electroanatomic mapping system (NOGA XP, Biologic Delivery Systems, Division of Biosense Webster, a Johnson&Johnson Company, Irwindale, California) and the navigator and mapping method have been described previously<sup>1</sup>. Briefly, unipolar and bipolar electrograms and the corresponding spatial positions of the tip of the catheter were recorded at about 200 equally distributed LV endocardial points and about 100 RV endocardial points, as well as about 50 points in the coronary sinus and veins, which represent a limited left epicardial surface. The sequentially recorded intracardiac electrogram and position data were temporally aligned using the simultaneously recorded 12-lead ECG. For the three-dimensional (3D) reconstruction of each mapped chamber during the acquisition process, the geometric filling threshold was set at 10 mm to reduce artificial interpolation. Points were

accepted by the system according to a set of criteria to evaluate catheter stability and signal quality.

### Construction of the anatomical models

Patient anatomies were semi-automatically reconstructed from the CMR images. Surfaces of relevant anatomical structures were constructed from their contours using Blender (The Blender Foundation). The outline of the ventricles was detected from short-axis cine images. Atrial cavities, aorta, major veins and outflow tracts were traced from FLASH sequences. Torso, lungs and electrode locations were segmented from an ultra-fast GRE dataset. Scarred tissue was inferred from LGE-MRI sequence by manual contour and alignment. The cardiac anatomy was eventually discretized into a 1-mm resolution grid. Ventricular fiber orientation was assigned using a rule-based approach. A 0.6-mm thick fast conducting layer was included in both left and right ventricular endocardium.

### Activation model

The ventricular electrical activation  $\tau(x)$  originated from selected locations, the early activation sites (EASs), located at  $x = s_i$  with onset of activation at time  $t_i$ , and spread across the myocardium with given spatially-varying, direction-dependent conduction velocity encoded in a tensor  $\mathbf{D}(x)$ . Mathematically, we modelled the activation with the eikonal equation which reads

$$\begin{cases} \sqrt{\mathbf{D}(x) \nabla \tau \cdot \nabla \tau} = 1, \\ \tau(s_i) = t_i. \end{cases}$$

The conduction tensor was set as

$$\mathbf{D} = \frac{\theta^2}{\beta} \mathbf{G}_{\text{in}} (\mathbf{G}_{\text{in}} + \mathbf{G}_{\text{ex}})^{-1} \mathbf{G}_{\text{ex}}$$

where  $\beta$  was the myocyte surface-to-volume ratio,  $\theta = 2.1$ , and  $\mathbf{G}_{\text{in}}$  and  $\mathbf{G}_{\text{ex}}$  were respectively the intra- and extra-cellular electric conductivity. In order to mimic the Purkinje network, a thin rapidly conducting layer was included along LV and RV endocardium, with a different value of  $\beta$ . Scars (taken from CMR imaging) were modeled as non-conductive area, with no border zone.

### Lead fields computation and ECG formula

For the computation of the ECG we used the following formula:

$$V_k(t) = U' * w = \int_0^\infty U'(t - \xi) w_k(\xi) d\xi$$

The function  $U(t)$  was the transmembrane potential as obtained from the Ten Tusscher-Panfilov ionic model.<sup>2</sup> The function  $w_k(t)$  represented the QRS complex obtained with the oblique dipole layer formulation:<sup>3</sup>

$$w_k(t) = \int_{S(t)} \mathbf{G}_{\text{in}} \mathbf{n} \cdot \nabla Z_k \, d\sigma$$

where  $\mathbf{G}_{\text{in}}$  was the intracellular conductivity tensor,  $S(t)$  the activation front with normal  $\mathbf{n}$  pointing towards the depolarized region, and  $Z_k(x)$  the lead field function for the lead  $k = 1, \dots, 12$ . Each lead field function  $Z_k(x)$  represented one of the 12 leads in the ECG.<sup>4</sup>

### Identification of early activation sites

The following parameters were considered in the optimization procedure: number  $N$ , location  $s_i$  and onset  $t_i$  of the EASs; a global myocyte surface-to-volume ratio  $\beta$ ; a local scaling  $r_l$  of the surface-to-volume ratio in 4 distinct regions (LV and RV myocardium, and LV and RV fast endocardial layer). The total number of free parameters was therefore variable and depending on the number of EASs. The initial value for  $\beta$  was  $1000 \text{ cm}^{-1}$ , while  $r_l$  was set to unity. The other parameters for the eikonal model and the lead fields were set accordingly to previous studies, being the same for all the patients.<sup>5</sup>

The first phase of the construction of the patient-specific models aimed at identifying an optimal set of early activation sites (EASs) and a global CV. Given the activation map  $\tau_i(x)$  at location  $x$  from each tentative EAS, we represented the combined activation map  $\tau(x)$  at location  $x$  in the following way:

$$\tau(x; t_1, \dots, t_n, \alpha, \beta) = \alpha \cdot \min\{\tau_1(x) + t_1, \dots, \tau_n(x) + t_n\} + \beta$$

for a set of unknown parameters  $(t_1, \dots, t_n, \alpha, \beta)$ , to be estimated. The formula for  $\tau(x)$  represents the simultaneous activation of  $n$  EASs each activating at time  $t = t_i$  and then affinely transformed. We remark that  $\tau(x)$  is still a solution of the eikonal equation, but its evaluation only required a fraction of the total cost (only the ECG needs to be recomputed.) The optimization of the free parameters to minimize the mismatch between recorded and simulated ECG was achieved by iterating the following steps:

1. Optimize  $(t_1, t_2, \dots, t_n)$  for fixed  $n, \alpha, \beta$ .
2. Optimize  $(\alpha, \beta)$  for fixed  $n, t_1, \dots, t_n$ .
3. Remove EASs whose region of influence was small (below 1% of the total volume.)

For the optimization we used the BOBYQA algorithm.<sup>6</sup> In the third step, we removed EASs by setting  $t_i = \infty$  in the combined activation map. In Figure 1 and Figure 2 we illustrate the

rationale of the first phase. All simulations were performed on a workstation equipped with an NVIDIA GeForce GTX-1080 card.

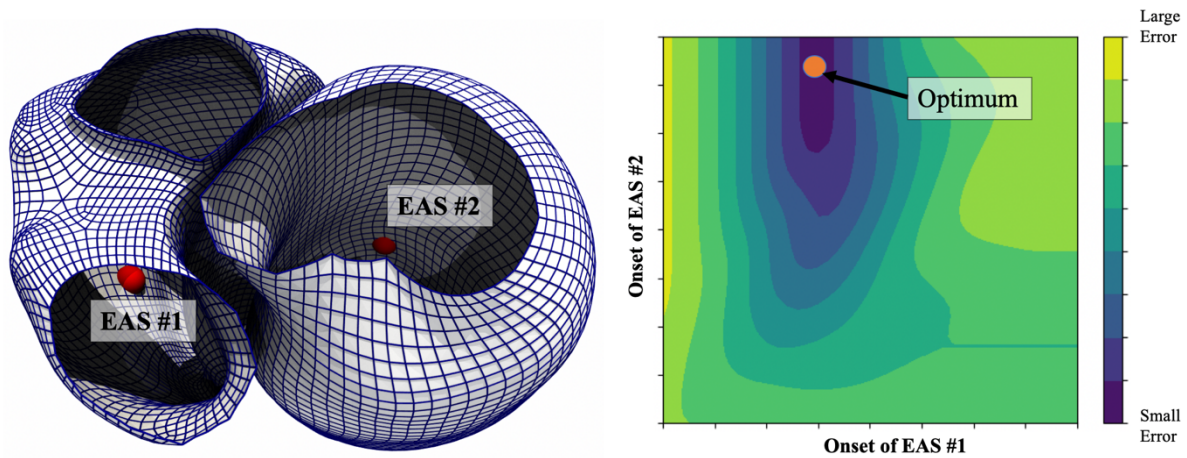


Figure 1. Illustrative example of the first optimization phase. We consider only 2 EASs, one placed on the RV endocardium, the other on the LV endocardium. We then evaluated the error between recorded and simulated ECG for several combinations of onsets (right plot). The optimal error (here unique) is for very late activation of EAS #2 and early activation of EAS #1, probably indicating a left bundle branch block.

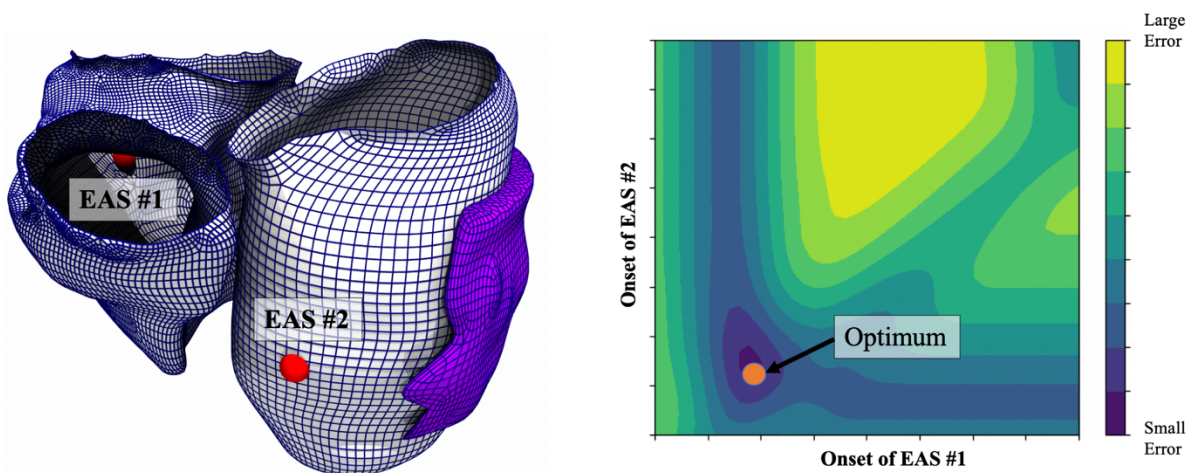


Figure 2. Illustrative example of the first optimization phase for a patient with scar and without a bundle branch block. The procedure is as the previous figure. In this case, the optimal onset indicates that both points activate early.

## Parametrization of endocardial surface and bull's-eye plot

Segmented LV and RV endocardium were parametrized with a global coordinate system to facilitate the localization of EASs and the visualization of endocardial activation (bull's-eye plots). Every 3-D point of the surface with canonical coordinates  $(x, y, z)$  was mapped to 2-D “texture” coordinates  $(u, v)$  within a circle of unit radius. In this way, the possibly complex endocardial surface was represented by the unit circle. An EAS on the surface was similarly mapped onto the unit circle.

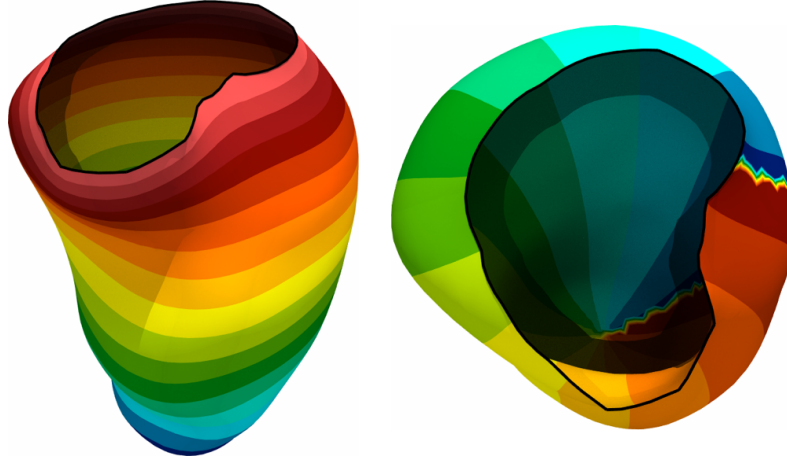


Figure 3. Example of the parametrization of the LV endocardium. On the left, the radial coordinate in the texture space, that is  $u^2 + v^2$ , on the right the rotational coordinate.

The parametrization was based on a previously proposed method, with minor modifications.<sup>7</sup> In our case, we only parametrized the endocardial surfaces and not the whole myocardium. We automatically identified the outer boundary of the surface (the valve ring) and mapped this curve to the unit circumference, with  $u = \cos(2\pi s)$  and  $v = \sin(2\pi s)$ , being  $s$  the curvilinear coordinate of the boundary. Then, we harmonically extended the boundary data to the whole surface, that is  $\nabla^2 u = 0$  and  $\nabla^2 v = 0$  with the above boundary data. This parametrization is generally not uniform across the surface, in the sense that an infinitesimal square in the texture space is typically mapped to a larger square when it is close to the apex rather than close to the base. Therefore, we recomputed the parametrization by solving the problem

$$\nabla \cdot (\mathbf{G}^{-1} \nabla w) = 0, \mathbf{G} = \left( \frac{\partial \mathbf{X}}{\partial w} \right)^T \left( \frac{\partial \mathbf{X}}{\partial w} \right), \mathbf{X} = [x, y, z]^T \text{ and } w = [u, v]^T.$$

The bull's-eye plot was defined as the representation of the LV endocardial surface in the texture space, since  $u^2 + v^2 \leq 1$ . This may slightly differ from other bull's-eye representations, which are generally based on a projection onto a prolate spheroid aligned with the LV.

### Interpolation of recorded activation map

In the LV and RV endocardium, a radial basis function regression method with multiquadric functions was employed to interpolate the recorded activation map in the full surface from acquired locations.

## Robustness of validation

In the recorded data, an uncertainty in the spatial location of [electroanatomic mapping \(EAM\)](#) points (2 mm) and in the detected activation time (4 ms) was assumed. With a Monte Carlo approach (10'000 samples) we perturbed the recorded EAM points with Gaussian noise using the above variances and repeated the evaluation of [breakthrough-point \(BP\)](#) location. Below we report the distribution of localization error for patient #1 in the case of BP evaluated as the barycenter of the earliest activated region (10% of total activation), versus the case when BP is simply the earliest activated point of the mesh. This analysis showed that

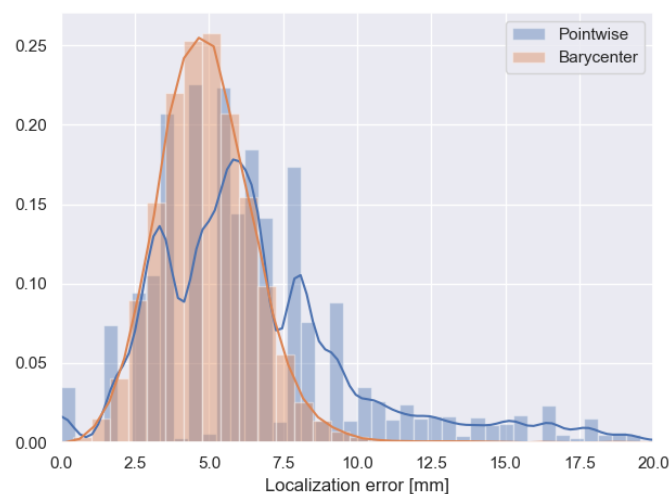


Figure 4. Distribution of localization error of BP with two different methods to identify the BP.

our definition of BP (and LAP) is more robust to uncertainty.

## References

- Potse M, Krause D, Kroon W, Murzilli R, Muzzarelli S, Regoli F, *et al.* Patient-specific modelling of cardiac electrophysiology in heart-failure patients. *Europace* 2014;**16**:iv56–61.
- [Ten](#) Tusscher KHWJ~~ten~~, Panfilov A-V. Alternans and spiral breakup in a human ventricular tissue model. *Am J Physiol Heart Circ Physiol* 2006;**291**:H1088–100.
- Colli Franzone P, Pavarino LF, Scacchi S. Mathematical Cardiac Electrophysiology. Cham: Springer International Publishing; 2014.
- Potse M. Scalable and Accurate ECG Simulation for Reaction-Diffusion Models of the Human Heart. *Front Physiol* 2018;**9**.
- Pezzuto S, Kal’avský P, Potse M, Prinzen FW, Auricchio A, Krause R. Evaluation of a

144 Rapid Anisotropic Model for ECG Simulation. *Front Physiol* 2017;**8**:265.

145 6. Powell MJD. The BOBYQA algorithm for bound constrained optimization without  
 146 derivatives. Dep. Appl. Math. Theor. Physics, Cent. Math. Sci. Wilberforce Road,  
 147 Cambridge CB3 0WA, England. 2009.

148 7. Bayer J, Prassl AJ, Pashaei A, Gomez JF, Frontera A, Neic A, *et al.* Universal  
 149 ventricular coordinates: A generic framework for describing position within the heart  
 150 and transferring data. *Med Image Anal* Elsevier; 2018;**45**:83–93.

151